A Comparison of Eight Transposition Models Applied for Different Orientations Under Different Albedo Scenarios

João Victor F. F. de Medeiros[1], Lucas Barboza[1], Janis Galdino[1], Diego Miranda[1], Olga Vilela[1], Emerson Gomes[1], Alex Pereira[2], Eduardo Jatoba[2], Alcides Neto[2], José Bione de Melo Filho[2]

[1] Center of Renewable Energy/Federal University of Pernambuco (CER-UFPE), Recife (Brazil)

[2] Hydroelectric Company of São Francisco (CHESF), Recife (Brazil)

Abstract

The simulation of photovoltaic and thermal systems requires accurate knowledge of the solar radiation incident on the plane of photovoltaic modules or thermal collectors. When irradiance in the tilted plane is not measured, transposition models are used to transpose the measurements from the horizontal plane to the plane of the array. In this work, eight models have been evaluated for four different orientations for a low-latitude city at a minute resolution, providing a better description of the radiation behavior. Three scenarios of albedo have been assessed for all orientations. A statistical comparison has been performed using normalized mean bias error, normalized root mean square error, the coefficient of determination, and a skill score (SS4) for the total solar radiation on a tilted plane. The Hay and Davies, Reindl, Muneer and Perez models presented the best results for Petrolina, Brazil (latitude 9.11ºS), where the sophisticated model of Perez presented the lowest values of nRMSE and highest values of R^2 and SS4 for all orientations. The detailed albedo analysis of the Petrolina soil indicated an average albedo of 27.72%, with higher data concentration between 25.52% and 27.80%. It was also observed that simulations conducted with albedo varying as a function of solar zenith angle or albedo considered constant, but based on local measurements, led to more accurate results than simulations conducted with constant albedo and indicated as default by commercial software for the soil in the region.

Keywords: Transposition models; Diffuse irradiance modeling; Inclined surfaces; Ground reflectance; semi-arid.

1. Introduction

The simulation of photovoltaic (PV) and thermal systems requires accurate knowledge of the solar radiation incident on the plane of PV modules or thermal collectors. Generally, the photovoltaic or thermal arrays are not installed horizontally, thus requiring transposition models. These models compute the global irradiance in the tilted plane as the sum of the direct, diffuse, and reflected irradiance from the ground (albedo). A simple geometric transformation is applied to the direct component. The reflected irradiance is estimated similarly, adding the influence of the ground type. The main difference between the transposition models is the approach to transposing the diffuse component, where two main groups are highlighted: 1) isotropic models, which consider only isotropic radiation; 2) anisotropic models, which add circumsolar and/or horizon brightness component into the analysis (García et al., 2021).

As the estimation models are strongly affected by the location's latitude due to site-specific characteristics and the stochastic nature of solar radiation, it is imperative to find the most accurate model for each site (Maleki et al., 2017). It is essential to evaluate the transposition models for different albedo scenarios, bearing in mind the advancing market for bifacial modules, and to evaluate those models for higher temporal resolution since data recording has been moved from hourly to a sub-hourly resolution to provide more information in the simulations (Gueymard and Ruiz-Arias, 2016). Moreover, the growth of solar energy has led to a massive increase in photovoltaic systems with different inclinations and orientations typically following the building construction aspects, notably BIPV (Building Integrated Photovoltaics) (Assoa et al., 2020).

In this context, the present work aims to investigate the performance of 8 widely used models to estimate total solar radiation on tilted surfaces with 1-minute measurements at Petrolina (Brazil) for four different orientations, north-, south-, east- and west-facing surfaces tilted at 45º. All models were evaluated in three different scenarios, with constant albedo and equal to 20%, average albedo measured at Petrolina and albedo varying as a function of the solar zenith angle. In addition, a detailed analysis of the local surface albedo was performed. The proposed study is performed within the framework of the R&D project "*Solar Platform of Petrolina - Development, Research and Innovation in Advanced Technologies*" (CHESF-ANEEL).

Selection and/or peer review under responsibility of Scientific Committee
doi:10.18086/eurosun.2022.15.11 Available at http://proceedings.ises.org

2. Transposition Models

The global tilted irradiance (GTI) can be estimated by the sum of the direct and diffuse irradiance incident on the inclined plane plus the irradiance reflected by the ground seen by the photovoltaic (PV) array. The GTI is thus calculated by the expression:

$$GTI = DNI * \cos(AI) + DHI * SVF + RHI * GVF \quad \text{(eq. 1)}$$

The direct irradiance incident on the tilted plane can be obtained from a simple geometric transformation, where the direct normal irradiance (DNI) component is multiplied by the cosine of the angle of incidence (AI). The diffuse portion is obtained by the product of diffuse horizontal irradiance (DHI) and the sky view factor (SVF). The irradiance reflected by the ground that is seen by PV array can be obtained by the reflected horizontal irradiance (RHI) multiplied by the ground view factor (GVF). The RHI is the product of global horizontal irradiance (GHI) and the ground reflectance (ρ_g), also called albedo (see equation 2).

$$\rho_g = RHI/GHI \quad \text{(eq. 2)}$$

Ground reflectance (albedo) is known to vary with several factors, such as the nature of the ground surface, solar zenith angle, specularity, cloud cover, presence or absence of snow, and other factors (Thevenard et al., 2006). Dirmhirn and Eaton (1975) showed that water and snow reflection can be forward-augmented or backward-augmented. Since the evaluated ground is predominantly composed of sandy soil, the albedo analysis will be based on the isotropic reflection of radiation.

Among the three components in the calculation of GTI, diffuse irradiance is the most difficult to compute because it strongly depends on the cloudiness and clearness conditions of the atmosphere (Duffie and Beckman, 2013). Several authors have studied this component from different approaches, from isotropic models that consider only the isotropic diffuse (Badescu, 2002; Koronakis, 1986; Liu and Jordan, 1961), to more complex and elaborated models that treat the circumsolar diffuse and/or the horizon brightness in more detail, called anisotropic models (Hay and Davies, 1980; Klucher, 1979; Perez et al., 1990; Reindl et al., 1990). All these models evaluate the sky view factor (SVF) between the collecting surface and the visible part of the sky.

The isotropic model proposed by Liu and Jordan (1961) [LJ] considers an isotropic distribution of diffuse radiation, with the diffuse irradiance incident on the sloping surface being given by DHI corrected by a sky view factor, represented by $(1 + \cos \beta)/2$. In Koronakis (1986) [Ko], a correction in Liu and Jordan's geometric factor is proposed, being corrected to $(2 + \cos \beta)/3$. In Badescu (2002), a 3D approach is performed and compared to the isotropic model of Liu and Jordan (1961), showing that Badescu's model estimation with SVF of $(3 + \cos 2\beta)/4$ was slightly more accurate for surfaces with a low slope for a high latitude location. Table 1 presents all isotropic models considered in this study.

Tab. 1: Sky view factor of all isotropic models for comparative analysis.

Model	Code	Equation of sky view factor (SVF)
Liu e Jordan (1961)	LJ	$SVF_{LJ} = \frac{1 + \cos \beta}{2}$ (eq.3)
Koronakis (1986)	Ko	$SVF_{Ko} = \frac{2 + \cos \beta}{3}$ (eq.4)
Badescu (2002)	Ba	$SVF_{Ba} = \frac{3 + \cos(2\beta)}{4}$ (eq.5)

The model proposed by Hay and Davies (1980) considers isotropic diffuse radiation, and also the circumsolar radiation, which results from the scattering of solar radiation concentrated in the solar disk. In this model, the anisotropy index of Hay and Davies (F_{HD}) is used. In 1977, Temps and Coulson (1977) applied a correction factor for the isotropic diffuse in order to consider the brightness of the horizon. Based on this authors, Klucher (1979) modified this correction factor with a modulating function to describe an all-sky model. Similarly, Reindl et al. (1990) modified the model of Hay and Davies (1980), proposing the addition of the horizon brightening term. This model is commonly referred as HDKR in the literature (Duffie and Beckman, 2013) due to the contribution of the 3 papers in the development of this model, in this work Reindl et al. (1990), or HDKR, will be referred as Re.

Another anisotropic model widely used and studied in the literature is the Perez et al. (1990) model, where the isotropic, circumsolar and horizontal diffuse radiation are analyzed more in detail. In this model coefficients representing solid angles of the circumsolar region are used (coefficients a_1 and a_2). In addition, empirical functions of sky brightness describing circumsolar radiation (F_1) and horizon brightness (F_2) are used considering air mass (m), normal incident extraterrestrial radiation (DNI_{ext}) and zenith angle (θ_z).

In the same year as Perez's model, Muneer (1990) proposes a model that discerns between overcast and non-overcast sky conditions, equation 11 presented in Table 2, relates the diffuse from an inclined surface to DHI, where for a tilted surface on a cloudy day, F_{HD} becomes zero and the term T becomes a ratio between the irradiance of a tilted surface and the diffuse horizontal irradiance. T corresponds to a function of the radiation distribution (b) and the surface slope (β) for a given location, so the parameters of equation 13 are adjusted as a function of the location evaluated. Table 2 presents the sky view factors for all anisotropic models evaluated in this work.

Tab. 2: Anisotropic models selected for comparative analysis.

Model	Code	Equation of sky view factor (SVF)
Klucher (1979)	Klu	$SVF_{Klu} = \left(\frac{1+\cos\beta}{2}\right)\left(1+F\sin^3\left(\frac{\beta}{2}\right)\right) * [1+F\cos^2 AI \sin^3(90-\alpha)]$ (eq.6) *where F is the modulating function of Klucher*: $F = 1-\left(\frac{DHI}{GHI}\right)^2$ (eq.7)
Hay and Davies (1980)	HD	$SVF_{HD} = \left[(1-F_{HD})\left(\frac{1+\cos\beta}{2}\right)+F_{HD}R_b\right]$ (eq.8) *where F_{HD} is the anisotropy index of HD and R_b is the geometric factor*: $F_{HD} = \frac{DNI}{DNI_{ext}}$ (eq. 9) $R_b = \frac{\cos AI}{\cos(\theta_z)}$ (eq. 10)
Muneer (1990)	Mu	$SVF_{Mu} = T(1-F_{HD})+F_{HD}R_b$ (eq.11) *where*: $T = \cos^2\frac{\beta}{2}+\frac{2b}{\pi(3+2b)}\left[sin\beta-\beta\cos\beta-\pi\sin^2\frac{\beta}{2}\right]$ (eq.12) *for the globe*: $\frac{2b}{\pi(3+2b)} = 0.04-0.82F_{HD}-2.026{F_{HD}}^2$ (eq.13)
Reindl *et al.* (1990)	Re	$SVF_{Re} = \left[(1-F_{HD})\left(\frac{1+\cos\beta}{2}\right)*\left(1+f\sin^3\left(\frac{\beta}{2}\right)\right)+F_{HD}R_b\right]$ (eq.14) *where f is the modulation factor of Reindl*: $f = \sqrt{\frac{DNI\cos\theta_z}{\mathrm{GHI}}}$ (eq.15)
Perez *et al.* (1990)	Pe	$SVF_{Pe} = \left[\left(\frac{1+\cos\beta}{2}\right)(1-F_1)+F_1\frac{a_1}{a_2}+F_2\sin\beta\right]$ (eq.16) *where*: $a_1 = \max(0,\cos AI)\,;\, a_2 = \max(\cos 85\,,\cos\theta_z)$ (eq.17) $F_1 = \max\left\{0,\left[\mathrm{F}_{11}+F_{12}\Delta+F_{13}\theta_z\left(\frac{\pi}{180}\right)\right]\right\};F_2 = \left[\mathrm{F}_{12}+F_{22}\Delta+F_{23}\theta_z\left(\frac{\pi}{180}\right)\right]$ (eq.18) $\Delta = m\frac{DHI}{DNI_{ext}}\;;m = \frac{1}{\cos\theta_z}$ (eq.19) *Where the coefficients contained in the equations of F_1 and F_2 are obtained based on the discrete categories of sky brightness (ε), with κ equal to 1.041 and θ_z in radians.* $\varepsilon = \frac{\frac{DHI+DNI}{DHI}+\kappa\theta_z^3}{1+\kappa\theta_z^3}$ (eq.20)

3. Experimental setup

The solarimetric station was installed in Petrolina, Brazil (latitude 9.11ºS, 40.44W) with four LI-COR Li-200R photovoltaic solarimeters disposed at 45º to the North, South, East, and West orientations. Two photovoltaic solarimeters were also arranged to measure the global horizontal irradiance (GHI) and the reflected horizontal irradiance (see Figure 1) to measure the ground albedo. All sensors were previously and periodically calibrated with a Kipp & Zonen CMP22 secondary standard pyranometer. According to Köppen classification, the climate in Petrolina is considered semi-arid (BSh).

Fig. 1: Solarimetric station installed at Petrolina, Brazil.

Based on GHI, DNI and DHI data measured with EKO class A pyranometers (model MS-80) and pyrheliometer (model MS-57), eight transposition models were evaluated using 1-min data measured between December 04, 2021, to April 29, 2022. A quality control procedure was applied to the measured radiation data to identify and remove outliers. The methodology applied is described in Petribú et al. (2017), and this data quality procedure consists of applying objective and automatic tests that can be divided into two large groups: global tests, which identify anomalies in the timestamps of the analyzed series, assessing the quality of the time series as a whole, and local tests, which are specific for each analyzed variable and take into account the physical nature of the variables studied. Following this methodology, the measurements corresponding to solar elevations below 7º were discarded.

The models were assessed for three scenarios: (i) one with albedo considered constant and equal to 20%, which is the default value adopted in commercial software for the local soil, (ii) albedo constant and equal to the average value of the ground reflectance, and the third scenario, (iii) evaluating the transposition models with albedo (ρ_g) varying as a function of solar zenith angle (θ_z). The evaluation was performed at the minute resolution using three isotropic models, Liu and Jordan (LJ), Koronakis (Ko) and Badescu (Ba), and five anisotropic models, Klucher (Klu), Hay and Davies (HD), Reindl (Re), Muneer (Mu) and Perez (Pe).

The accuracy of the estimates for the global tilted irradiance is assessed using the usual error metrics, the normalized mean bias error (nMBE), the normalized root mean square error (nRMSE) and the coefficient of determination (R^2) defined in equations 21 to 23.

$$nMBE = \frac{1}{N\,\bar{x}_{meas}} \sum_{i=1}^{N} (x_{sim}^{i} - x_{meas}^{i}) \qquad \text{(eq. 21)}$$

$$nRMSE = \frac{1}{\bar{x}_{meas}} \sqrt{\frac{1}{N}\sum_{i=1}^{N}(x_{sim}^{i} - x_{meas}^{i})^2} \quad \text{(eq. 22)}$$

$$R^2 = 1 - \frac{\sum_{i=1}^{N}(x_{sim}^{i} - x_{meas}^{i})^2}{\sum_{i=1}^{N}(x_{sim}^{i} - \bar{x}_{meas}^{i})^2} \quad \text{(eq. 23)}$$

where N is the number of observations data, x_{meas}^{i}, $\bar{x}_{meas}$, and x_{sim}^{i} correspond, respectively, to the measured irradiance at moment *i*, the average value of the observations (measured) and the simulated irradiance obtained by the models at instant *i*.

The nMBE indicates how much the model underestimates or overestimates the results with respect to real measured data. When nMBE is negative, the model underestimates the measured values. nRMSE indicates the dispersion of the data. A model with a low nRMSE compared to the others, indicates that this model best fits the observational data. The R^2 quantifies the variance between the observational data and the estimated data; the closer it is to 1, the better the observed data is replicated by the model.

In addition, a skill score (SS4) which indicates the overall performance of a model, was selected to rank all models. This statistical presented in equation 24 considers correlation (R) and the standard deviation of a model (std_{mod}) normalized by the *std* of the observation (std_{obs}) (Taylor, 2001). Similar to the coefficient of determination, SS4 is a statistic that ranks the model from zero to one, being from worst to best quality, respectively.

$$SS4 = \frac{(1+R)^4}{4\left(\frac{std_{mod}}{std_{obs}} + \frac{1}{std_{mod}/std_{obs}}\right)^2} \quad \text{(eq. 24)}$$

4. Results and discussion

Since the comparative analysis of the transposition models in this work deals with the albedo for three different scenarios, the albedo is initially evaluated in order to calculate the average albedo of the ground (for scenario ii), and to evaluate the variation of the surface reflectance as a function of solar position, described by the zenith angle, scenario (iii). Scenario (i) assumes an albedo equal to 20%.

4.1. Albedo Evaluation

The early and late hours of the day, in other words, times when the Sun has low elevation and thus high zenith angle, tend to have higher albedos values than those observed at midday, this variation is explained in Marion (2020) due to the distribution of the solar spectrum shifting to longer wavelengths for these times. In addition, the albedo may increase due to the angle of incidence of the radiation on the surface being increased (Marion, 2020). The observed variation of the Petrolina ground reflectance is presented in Fig. 2. Note that the soil is predominantly sandy as observed in Fig. 1.

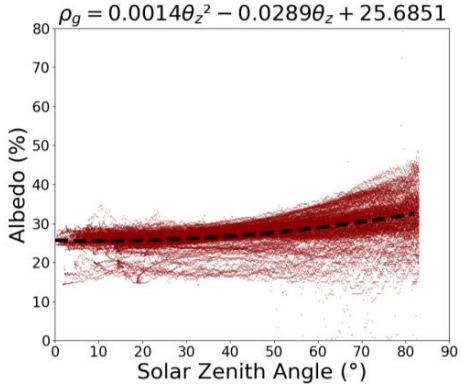

Fig. 2: Albedo as a function of solar zenith angle.

This upward profile is observed in other works, which relate both variables, in linear form (Lave et al., 2015), or from polynomial equations (Wang et al., 2005). Other works also relate albedo and solar elevation, applying exponential functions (Liu et al., 2008; Demain et al., 2013). From the data measured in Petrolina, a semi-arid region, albedo varies according to equation 25.

$$\rho_g = 0.0014\theta_z^2 - 0.0289\theta_z + 25.6851 \quad \text{(eq. 25)}$$

The highest concentration of albedo data is observed in the region above 25% (Fig. 3a). When evaluating the histogram (Fig. 3b) it is observed that this concentration of points is given for values between 25.52% and 27.80%, with the average albedo for the entire time series being 27.72%.

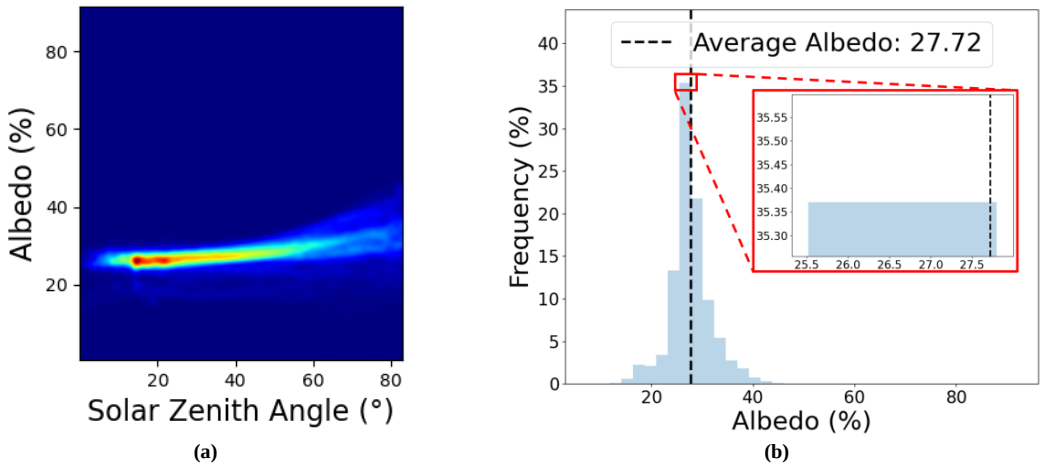

(a) (b)

Fig. 3: Distribution of albedo data observed by a) colormap and b) histogram.

4.2. Transposition Models

A comparative analysis between the transposition models was performed for the three scenarios. The value of 20% was considered for the first scenario because it is usually applied as a default value in commercial software. For this scenario, the results indicate better performance of Perez model, with lower nRMSE and higher R^2 and SS4 for all orientations evaluated, similar to Yang (2016) and García et al. (2021). The north and south orientations evaluated presented lower nRMSE than the solarimeters facing east and west. Despite the higher values of nRMSE for the east and west orientations, it is observed the same description of the models, where the Hay and Davies (HD), Reindl (Re), Muneer (Mu) and Perez (Pe) models were predominantly performant, with an emphasis on Perez's model. Tab. 3, 4 and 5 present the statistical metrics for the three scenarios adopted, i, ii and iii respectively. The four best models have been highlighted in **bold** for each of the statistics, and the best model for each metric has been **underlined**.

Tab. 3: Statistics of all 8 models for scenario i) albedo constant and equal to 20%.

	North				South				East				West			
Model	**nMBE (%)**	**nRMSE (%)**	**R^2 (-)**	**SS4 (-)**	**nMBE (%)**	**nRMSE (%)**	**R^2 (-)**	**SS4 (-)**	**nMBE (%)**	**nRMSE (%)**	**R^2 (-)**	**SS4 (-)**	**nMBE (%)**	**nRMSE (%)**	**R^2 (-)**	**SS4 (-)**
Ba	-5,81	17,01	0,953	0,948	-7,44	16,09	0,956	0,952	-7,23	20,00	0,948	0,940	-11,52	22,34	0,954	0,931
HD	**-1,93**	**15,25**	**0,956**	**0,954**	-2,85	**13,07**	**0,964**	**0,962**	-3,73	**16,54**	**0,958**	**0,958**	-7,05	**16,98**	**0,964**	**0,958**
Klu	3,41	15,93	0,953	0,953	**1,58**	13,37	0,960	0,961	3,36	16,64	0,957	0,957	**-2,31**	17,07	0,958	0,949
Kor	3,71	16,91	0,947	0,947	**1,49**	14,03	0,956	0,956	**2,05**	18,91	0,944	0,941	**-3,64**	20,03	0,945	0,928
LJ	**0,66**	16,14	0,950	0,948	**-1,37**	13,90	0,957	0,956	**-0,92**	18,60	0,946	0,942	**-6,17**	20,35	0,949	0,930
Mu	**1,27**	**15,08**	**0,957**	**0,957**	**0,16**	**12,94**	**0,963**	**0,963**	**-0,67**	**16,46**	**0,959**	**0,958**	**-4,42**	**15,57**	**0,964**	**0,962**
Pe	-2,20	**14,19**	**0,962**	**0,961**	-2,25	**12,56**	**0,966**	**0,966**	**-1,54**	**14,21**	**0,968**	**0,968**	-6,72	**15,25**	**0,972**	**0,967**
Re	**-1,10**	**15,23**	**0,956**	**0,954**	-2,06	**12,92**	**0,964**	**0,963**	-2,93	**16,44**	**0,958**	**0,958**	-6,37	**16,69**	**0,964**	**0,958**

Tab. 4: Statistics of all 8 models for scenario ii) albedo constant and equal to 27.72%.

	North				South				East				West			
Model	**nMBE (%)**	**nRMSE (%)**	**R² (-)**	**SS4 (-)**	**nMBE (%)**	**nRMSE (%)**	**R² (-)**	**SS4 (-)**	**nMBE (%)**	**nRMSE (%)**	**R² (-)**	**SS4 (-)**	**nMBE (%)**	**nRMSE (%)**	**R² (-)**	**SS4 (-)**
Ba	-4,35	16,40	0,953	0,950	-6,07	15,36	0,956	0,954	-5,80	19,48	0,947	0,941	-10,31	21,58	0,953	0,933
HD	**-0,47**	**14,92**	**0,957**	**0,956**	**-1,48**	**12,65**	**0,965**	**0,964**	-2,30	**16,18**	**0,959**	**0,959**	-5,84	**16,30**	**0,964**	**0,959**
Klu	4,87	16,36	0,953	0,953	2,96	13,68	0,961	0,961	4,79	17,12	0,957	0,956	**-1,10**	16,89	0,957	0,949
Kor	5,18	17,28	0,947	0,947	2,87	14,25	0,956	0,956	3,48	19,20	0,943	0,941	**-2,43**	19,77	0,944	0,929
LJ	**2,13**	16,20	0,950	0,949	**0,01**	13,79	0,957	0,957	**0,50**	18,63	0,945	0,942	**-4,96**	19,92	0,948	0,931
Mu	2,74	**15,30**	**0,957**	**0,957**	1,53	**13,09**	**0,963**	**0,963**	**0,76**	**16,59**	**0,959**	**0,958**	**-3,21**	**15,20**	0,964	**0,962**
Pe	**-0,74**	**13,93**	**0,963**	**0,962**	**-0,88**	**12,33**	**0,966**	**0,966**	**-0,11**	**14,09**	**0,968**	**0,968**	-5,51	**14,58**	**0,972**	**0,968**
Re	**0,37**	**15,01**	**0,956**	**0,956**	**-0,69**	**12,60**	**0,964**	**0,964**	**-1,51**	**16,18**	**0,959**	**0,959**	-5,15	**16,07**	**0,964**	**0,959**

Tab. 5: Statistics of all 8 models for scenario iii) albedo as a function of θ_z.

	North				South				East				West			
Model	**nMBE (%)**	**nRMSE (%)**	**R² (-)**	**SS4 (-)**	**nMBE (%)**	**nRMSE (%)**	**R² (-)**	**SS4 (-)**	**nMBE (%)**	**nRMSE (%)**	**R² (-)**	**SS4 (-)**	**nMBE (%)**	**nRMSE (%)**	**R² (-)**	**SS4 (-)**
Ba	-4,53	16,49	0,953	0,949	-6,24	15,46	0,956	0,953	-5,99	19,52	0,948	0,941	-10,47	21,68	0,953	0,932
HD	**-0,66**	**14,96**	**0,957**	**0,956**	-1,65	**12,70**	**0,965**	**0,964**	-2,49	**16,18**	**0,959**	**0,959**	-5,99	**16,38**	**0,964**	**0,959**
Klu	4,68	16,27	0,953	0,953	2,78	13,60	0,961	0,961	4,60	17,01	0,957	0,957	**-1,25**	16,91	0,957	0,949
Kor	4,99	17,19	0,948	0,947	2,69	14,17	0,956	0,956	3,30	19,10	0,944	0,941	**-2,58**	19,77	0,945	0,929
LJ	**1,94**	16,17	0,950	0,949	**-0,17**	13,77	0,957	0,957	**0,32**	18,57	0,946	0,942	-5,11	19,95	0,948	0,931
Mu	2,55	**15,23**	**0,957**	**0,957**	**1,36**	**13,03**	**0,963**	**0,963**	**0,57**	**16,50**	**0,959**	**0,958**	**-3,36**	**15,23**	0,964	**0,962**
Pe	**-0,92**	**13,96**	**0,962**	**0,962**	**-1,05**	**12,35**	**0,966**	**0,966**	**-0,29**	**14,08**	**0,968**	**0,968**	-5,66	**14,68**	**0,972**	**0,968**
Re	**0,18**	**15,02**	**0,957**	**0,955**	**-0,87**	**12,63**	**0,964**	**0,964**	**-1,69**	**16,16**	**0,959**	**0,959**	**-5,31**	**16,15**	**0,964**	**0,959**

Similar to García et al. (2021), anisotropic models (HD, Klu, Mu, Pe and Re) presented better results than isotropic models (LJ, Ko and Ba) by better fitting the experimental data. It was also observed that simulations conducted with albedo varying as a function of solar zenith angle or albedo considered constant, but based on local measurements, led to more accurate results than simulations conducted with constant default albedo equal to 20%. This fact is valid for the models that underestimated the observational data, Badescu (2002), Hay and Davies (1980), Perez et al. (1990) and Reindl et al. (1990). These models presented negative nMBE for scenario i (albedo = 20%), as presented in Table 2. When the albedo adjustment was performed (scenarios ii and iii), considering the locally measured data (average albedo) and the variable albedo, a reduction in bias was observed for these models, as well as an improvement in the nRMSE. As an example, it can be seen the reduction in nRMSE for the Perez model with North orientation, the nRMSE is 14.19% with constant albedo (0.20), while the simulation with variable albedo resulted in the reduction of this statistical metric (13.96%).

Moreover, from Tab. 4 and Tab. 5, it can be seen that the input in the estimation of the global tilted irradiance with the local average albedo does not substantially impact R^2 and SS4 when compared to the simulations that consider the variable albedo. However, it tends to have better bias and better dispersion of the estimated data, thus leading to slightly better performance. In Nygren and Sundström (2021), photovoltaic systems with bifacial modules were evaluated for three albedo conditions, hourly variable albedo, fixed albedo and satellite-derived albedo. It was observed that for the modules' front face, the albedo type variation does not have a high impact. However, for the rear side, the simulations performed with variable albedo presented higher accuracy when compared to fixed albedo and satellite-derived albedo.

With the aim of facilitating the comparative analysis of the models, the Taylor diagram (Taylor, 2001) was adopted as a tool to evaluate the models against the measured results. Fig. 4 to Fig. 7 presents the diagrams for each orientation (north, south, east and west). Graphical statistical analysis is a valuable tool, where correlation, standard deviation, RMSE and SS4 are presented. The magenta color indicates the observed series and the dots indicate each model. The model that is closest to the magenta dot, indicated at the bottom of the graph, tends to describe the observational series best. Thus, models that are closer to the pink line and closer to the bottom of the frame highlighted in the figures, tend to have a better description of the observed data.

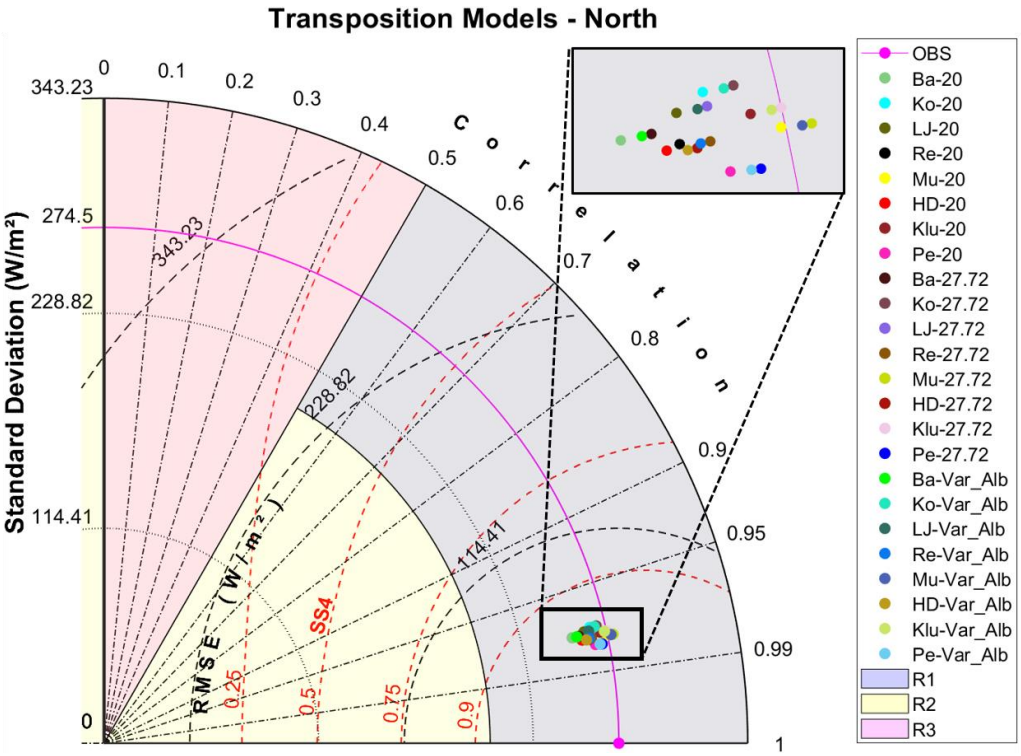

Fig. 4: Taylor diagram of all transposition models for North orientation (45º).

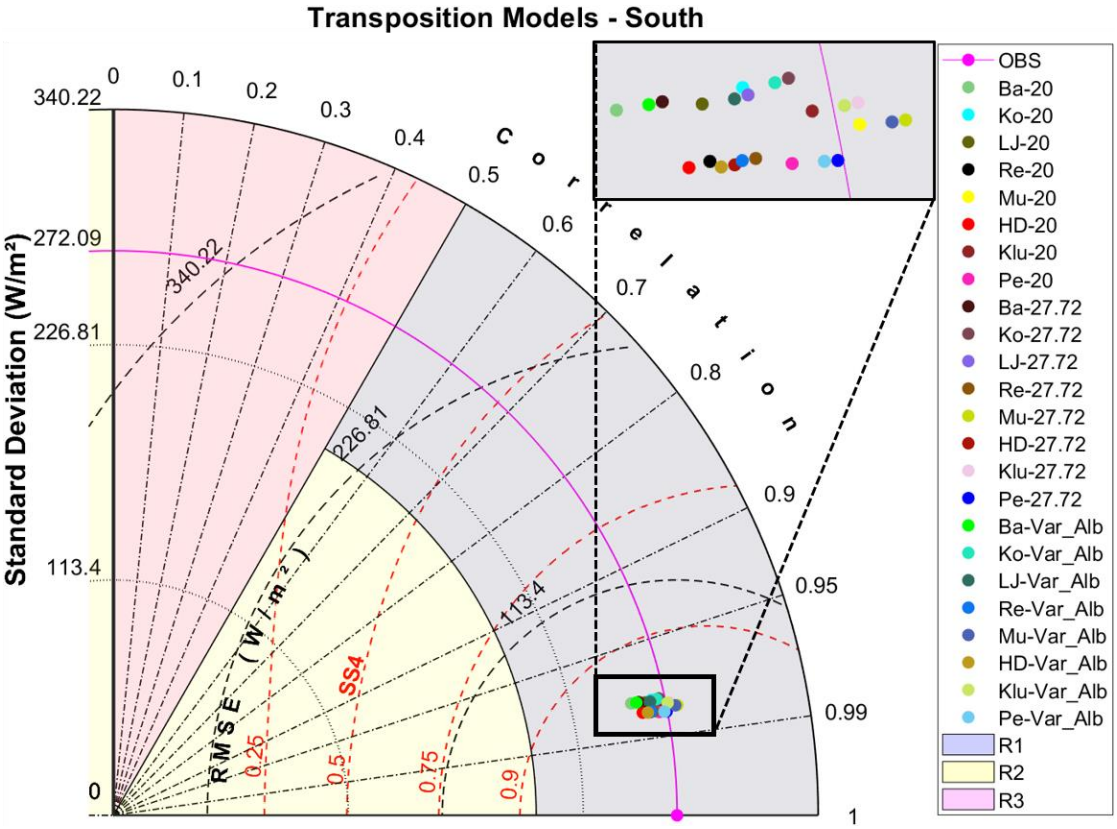

Fig. 5: Taylor diagram of all transposition models for South orientation (45º).

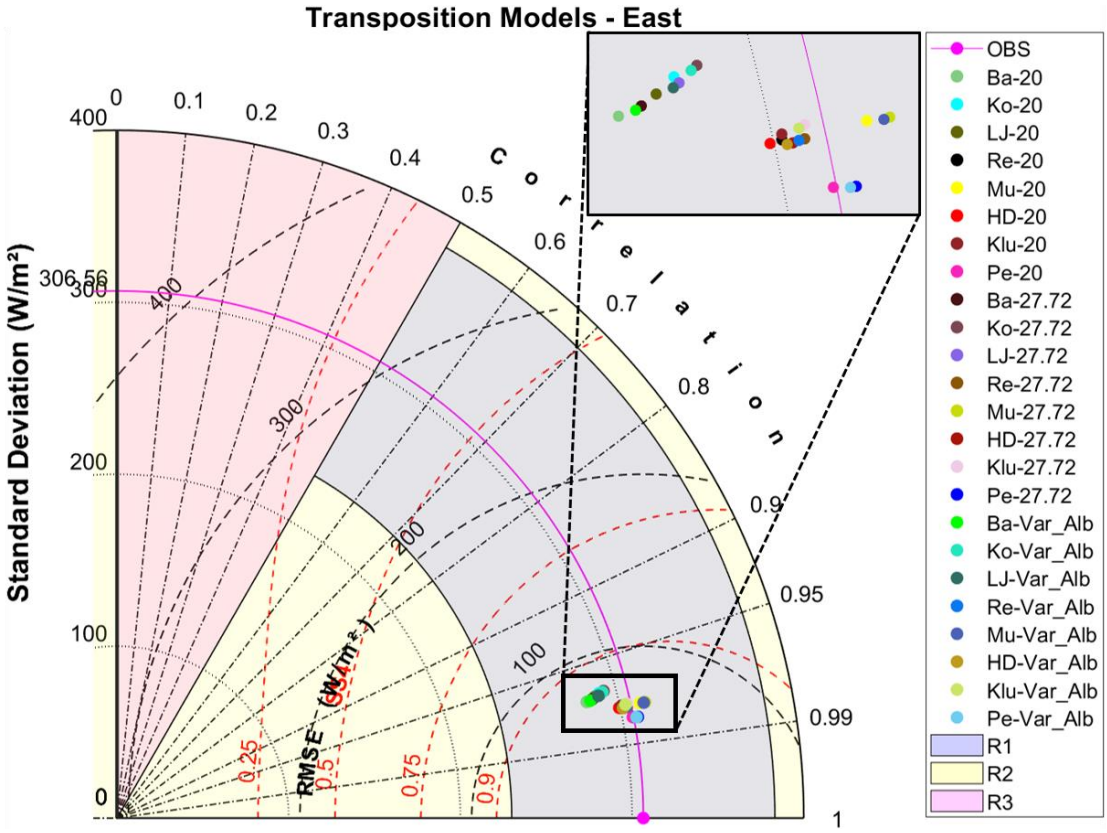

Fig. 6: Taylor diagram of all transposition models for East orientation (45°).

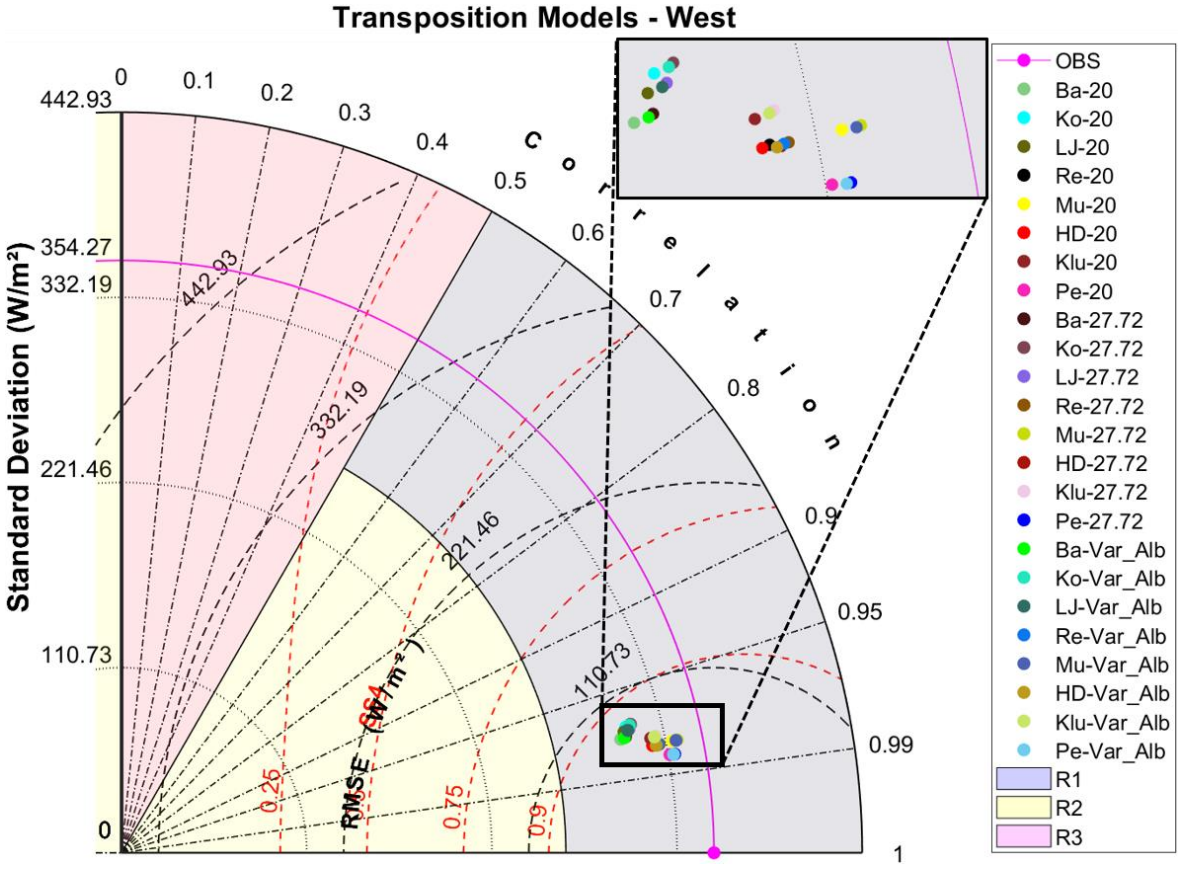

Fig. 7: Taylor diagram of all transposition models for West orientation (45°).

It can be observed from the graphs shown in Fig. 4 to 7 that the models do not present high differences between themselves. This fact may be linked to the climatic conditions of Petrolina because the DNI component has a high impact on GTI calculation. The modelling of the diffuse component does not have a powerful impact. However, although the differences are slight, it is observed that the Perez model tends to be closer to the magenta colour point (observation - OBS), presenting the best RMSE and SS4, thus demonstrating to be the best model for the location. The variation of the albedo scenarios, from constant albedo and equal to 20% for the two other scenarios, results in a slight difference between them. However, it improves the model performance from the Taylor skill score and the relationship between the standard deviations of the model with the observation for the North, South and West orientations.

It is worth noting that the present work evaluated the transposition models with measured DNI, DHI and GHI data as inputs. Applying GHI separation models at 1-min resolution may lead to even more variation in GTI calculations since DHI and DNI modelling can generate higher errors if the model employed does not fit the evaluated location (de Medeiros et al., 2022; Yang, 2022).

5. Conclusion

The present work investigated the performance of 8 models commonly used in the literature to estimate the radiation incident on tilted photovoltaic modules at Petrolina, Northeast region of Brazil. The results indicate that Hay and Davies, Reindl, Muneer, and Perez models presented the best performances, especially the Perez model that presented the best nRMSE and SS4 results for all orientations and scenarios evaluated.

Three albedo scenarios were considered to estimate the GTI irradiance, where it was observed that despite slight differences, the simulations conducted with the average albedo of the site resulted in greater accuracy. Furthermore, from the detailed analysis of the ground reflectance of Petrolina, an average albedo value corresponding to 27.72% was observed for the sandy soil type of Petrolina, with a higher concentration of data between 25.52% and 27.80% albedo values.

The graphical analysis of the Taylor diagram allowed a better visualization that the Perez model tends to be more in agreement with the observation, being able to describe the irradiance in the inclined plane better.

As future prospects, it is desired to evaluate the variable albedo for different sky conditions, assigning equations for cloudy sky, clear sky or partly cloudy sky, thus seeking to achieve more accurate simulations. Furthermore, it is intended to extend the analyses performed here, having as input data the results obtained by GHI separation models, to assess how the combination of separation + transposition models impacts the estimation of GTI irradiance.

6. Acknowledgments

The authors thank the financial support from the National Agency of Electric Energy (ANEEL) and Hydroelectric Company of São Francisco (CHESF) under the ANEEL R&D Program (CVI 23076.009704/2020-56). Likewise, the authors acknowledge the financial support provided by the Human Resources Training Program of the Brazilian National Agency for Petroleum, Natural Gas and Biofuels – PRH-ANP/FINEP, via PRH 48.1/UFPE (ANP Process number Nº48610.201019/2019-38), and to the Coordination for the Improvement of Higher Education Personnel (CAPES) in the scope of the graduate program of the UFPE members.

7. References

Assoa, Y.B., de Medeiros, J.V.F.F., Thony, P., 2020. Impact of Configurations on the Performance Prediction of Building Integrated Photovoltaic Modules. In EU PVSEC 2020, 37th European Photovoltaic Solar Energy Conference and Exhibition, pp. 1937-1940. https://doi.org/10.4229/EUPVSEC20202020-6CV.2.23.

Badescu, V., 2002. 3D isotropic approximation for solar diffuse irradiance on tilted surfaces. Renewable energy, 26(2), 221-233. https://doi.org/10.1016/S0960-1481(01)00123-9.

Demain, C., Journée, M. and Bertrand, C., 2013. Evaluation of different models to estimate the global solar radiation on inclined surfaces. Renewable energy, 50, pp.710-721. https://doi.org/10.1016/j.renene.2012.07.031.

de Medeiros, J.V.F.F., de Miranda, D.R., Gomes, E.T.A., Vilela, O.C., Pereira, A.C., Jatoba, E.B., de Melo Filho, J.B., 2022. Avaliação de modelos utilizados na estimativa da radiação difusa na resolução dos minutos para uma cidade de baixa latitude. In Congresso Brasileiro de Energia Solar-CBENS (pp. 1-10).

Dirmhirn, I., Eaton, F. D., 1975. Some characteristics of the albedo of snow. Journal of Applied Meteorology and Climatology, 14(3), 375-379. https://doi.org/10.1175/1520-0450(1975)014<0375:SCOTAO>2.0.CO;2.

Duffie, J. A., Beckman, W. A., 2013. Solar engineering of thermal processes, fourth ed. John Wiley & Sons.

García I., de Blas M., Hernández B., Sáenz C., Torres J.L., 2021. Diffuse irradiance on tilted planes in urban environments: Evaluation of models modified with sky and circumsolar view factors. Renewable Energy. 180, 1194-1209. https://doi.org/10.1016/j.renene.2021.08.042.

Gueymard, C.A., Ruiz-Arias, J.A., 2016. Extensive worldwide validation and climate sensitivity analysis of direct irradiance predictions from 1-min global irradiance. Solar Energy, 128, 1–30. https://doi.org/10.1016/j.solener.2015.10.010.

Hay, J. E., Davies, J. A., 1980. Calculation of the Solar Radiation Incident on an Inclined Surface. In: Proceedings of the First Canadian Solar Radiation Data Workshop. Ministry of Supply and Services, Toronto, Canada, 59.

Koronakis, P. S., 1986. On the choice of the angle of tilt for south facing solar collectors in the Athens basin area. Solar Energy, 36(3), 217-225. https://doi.org/10.1016/0038-092X(86)90137-4.

Klucher, T. M., 1979. Evaluation of models to predict insolation on tilted surfaces. Solar energy, 23(2), 111-114. https://doi.org/10.1016/0038-092X(79)90110-5.

Lave, M., Hayes, W., Pohl, A., & Hansen, C. W., 2015. Evaluation of global horizontal irradiance to plane-of-array irradiance models at locations across the United States. IEEE journal of Photovoltaics, 5(2), 597-606. https://doi.org/10.1109/JPHOTOV.2015.2392938.

Liu, B., Jordan, R., 1961. Daily insolation on surfaces tilted towards equator. ASHRAE J., 10.

Liu, H., Wang, B., Fu, C., 2008. Relationships between surface albedo, soil thermal parameters and soil moisture in the semi-arid area of Tongyu, northeastern China. Advances in Atmospheric Sciences, 25(5), 757-764. https://doi.org/10.1007/s00376-008-0757-2.

Maleki, S.A.M., Hizam, H., Gomes, C., 2017. Estimation of hourly, daily and monthly global solar radiation on inclined surfaces: Models re-visited. Energies, 10, 134. https://doi.org/10.3390/en10010134.

Marion, B., 2020. Albedo data sets for bifacial PV systems. In 2020 47th IEEE Photovoltaic Specialists Conference (PVSC) (pp. 0485-0489). IEEE. https://doi.org/10.1109/PVSC45281.2020.9300470.

Muneer, T., 1990. Solar radiation model for Europe. Building services engineering research and technology, 11(4), 153-163. https://doi.org/10.1177/014362449001100405.

Nygren, A., Sundström, E., 2021. Modelling bifacial photovoltaic systems: Evaluating the albedo impact on bifacial PV systems based on case studies in Denver, USA and Västerås, Sweden.

Perez, R., Ineichen, P., Seals, R., Michalsky, J., Stewart, R., 1990. Modeling daylight availability and irradiance components from direct and global irradiance. Solar energy, 44(5), 271-289. https://doi.org/10.1016/0038-092X(90)90055-H.

Reindl, D. T.; Beckman, W. A.; Duffie, J. A.. 1990. Evaluation of Hourly Tilted Surface Radiation Models. Solar Energy, 45(1), 9–17. https://doi.org/10.1016/0038-092X(90)90061-G.

Taylor, K.E., 2001. Summarizing multiple aspects of model performance in a single diagram. Journal of Geophysical Research: Atmospheres, 106, 7183-7192. https://doi.org/10.1029/2000JD900719.

Temps, R. C., Coulson, K. L., 1977. Solar radiation incident upon slopes of different orientations. Solar energy, 19(2), 179-184. https://doi.org/10.1016/0038-092X(77)90056-1.

Thevenard, D., Haddad, K., 2006. Ground reflectivity in the context of building energy simulation. Energy and buildings, 38(8), 972-980. https://doi.org/10.1016/j.enbuild.2005.11.007.

Yang, D., 2016. Solar radiation on inclined surfaces: Corrections and benchmarks. Solar Energy. 136. https://doi.org/10.1016/j.solener.2016.06.062.

Yang, D., 2022. Estimating 1-min beam and diffuse irradiance from the global irradiance: A review and an extensive worldwide comparison of latest separation models at 126 stations. Renewable and Sustainable Energy Reviews, 159, 112195. https://doi.org/10.1016/j.rser.2022.112195.

Wang, Z., Barlage, M., Zeng, X., Dickinson, R. E., Schaaf, C. B., 2005. The solar zenith angle dependence of desert albedo. Geophysical Research Letters, 32(5). https://doi.org/10.1029/2004GL021835.